

Building components for an outpost on the Lunar soil by means of a novel 3D printing technology

Giovanni Cesaretti ^a, Enrico Dini ^b, Xavier De Kestelier ^c, Valentina Colla ^{d,*}, Laurent Pambaguien ^e

^a Alta SpA, via A. Gherardesca 5, 56123 Pisa, Italy

^b Monolite Ltd., 101 Wardour Street, W1F 0UN, London, UK

^c Foster+Partners, Riverside, 22 Hester Road, SW11 4AN, London, UK

^d Scuola Superiore Sant'Anna, Istituto TeCIP, Laboratorio PERCRO, via Alamanni 13D, 56010 San Giuliano Terme, Pisa, Italy

^e ESA European Space Research and Technology Centre, Postbus 299, 2200 AG Noordwijk, The Netherlands

ARTICLE INFO

Article history:

Received 4 December 2012

Received in revised form

20 May 2013

Accepted 21 July 2013

Available online 8 August 2013

Keywords:

3D printing

Direct manufacturing

Lunar habitat

Human exploration

Regolith

Structural optimisation

ABSTRACT

3D-printing technologies are receiving an always increasing attention in architecture, due to their potential use for direct construction of buildings and other complex structures, also of considerable dimensions, with virtually any shape. Some of these technologies rely on an agglomeration process of inert materials, e.g. sand, through a special binding liquid and this capability is of interest for the space community for its potential application to space exploration. In fact, it opens the possibility for exploiting in-situ resources for the construction of buildings in harsh spatial environments. The paper presents the results of a study aimed at assessing the concept of 3D printing technology for building habitats on the Moon using lunar soil, also called regolith. A particular patented 3D-printing technology – D-shape – has been applied, which is, among the existing rapid prototyping systems, the closest to achieving full scale construction of buildings and the physical and chemical characteristics of lunar regolith and terrestrial regolith simulants have been assessed with respect to the working principles of such technology. A novel lunar regolith simulant has also been developed, which almost exactly reproduces the characteristics of the JSC-1A simulant produced in the US. Moreover, tests in air and in vacuum have been performed to demonstrate the occurrence of the reticulation reaction with the regolith simulant. The vacuum tests also showed that evaporation or freezing of the binding liquid can be prevented through a proper injection method. The general requirements of a Moon outpost have been specified, and a preliminary design of the habitat has been developed. Based on such design, a section of the outpost wall has been selected and manufactured at full scale using the D-shape printer and regolith simulant. Test pieces have also been manufactured and their mechanical properties have been assessed.

© 2013 IAA. Published by Elsevier Ltd. All rights reserved.

1. Introduction

The former idea of Moon colonisation originated far before the age of actual space exploration, as the Moon is

the only Earth's natural satellite. Recent discoveries of considerable amounts of water close to the Lunar poles as well as the need to optimise space exploration by exploiting Moon bases [1] and thus reducing the amount of fuel required for take-off (thanks to the fact that the Lunar gravity is far lower than the Earth's one) makes this opportunity more concrete and appealing [2–4]. However the establishment of a manned human colony on the Moon (or on Mars) will need some form of infrastructure to shelter the astronauts and scientific instrumentations

* Corresponding author. Tel.: +39 050 88 2507; fax: +39 050 88 2564.

E-mail addresses: g.cesaretti@alta-space.com (G. Cesaretti), enrico.dini@d-shape.com (E. Dini), xdekeste@FosterandPartners.com (X. De Kestelier), colla@sssup.it (V. Colla), Laurent.Pambaguien@esa.int (L. Pambaguien).

from a very harsh environment, which is surely characterised by deep vacuum conditions, strong temperature gaps, radiations and micrometeoroids. To this aim, the following different alternative options are under investigation:

- To dig the Lunar surface in order to build an underground habitat [5].
- To bring fully functional and complete habitation modules from Earth to be mounted on the Lunar surface.
- To design structures that can be directly built on the Moon surface using the local material, namely the Lunar soil.

From an historical point of view, namely if one considers what has been previously done by the newly established inhabitants during the colonisation of the different continents of our planet, the last solution is the more ‘natural’ one. The possibilities of modern space transports greatly progressed in recent years and a complex analysis is required to define the suitable trade-off allowing to point out most appropriate concept. Indeed, the construction of a lunar outpost through the exploitation of local material presents some evident advantages. With respect to the solution consisting in an extensive excavation of the Moon surface [5], much less material need to be manipulated, which implies considerable energy savings. Moreover the structure of the Moon geological system is not fully known and several explorative missions would be required to actually assess the feasibility and the eventual features of an underground outpost. On the other hand, if prefabricated and ready-to-use modules are exploited, the transport of large structures from Earth is required and many maintenance operation could not be performed on site. Furthermore, by exploiting local material, an efficient radiation shielding is achievable by manufacturing structures with a sufficient wall thickness.

The technical and strategic problems related to Moon colonisation are deeply examined in [6], where it has been underlined that the main issues to face for a Lunar outpost is clearly the long term human survival in its particular atmosphere, gravity and surface characteristics as well as strong temperature variations. Some general habitat concepts for a lunar or planetary surface structures are presented in [7] where also some important considerations to guide overall planning and element design are proposed, taking into account how the harsh environment affects on structures, devices and crews and how the scarcity of equipment as well as of human and consumable resources requires very stringent economies. The National Aeronautics and Space Administration (NASA) supported studies as well as simulations exploiting a Habitat Demonstration Unit (HDU) in a Pressurised Excursion Module (PEM) configuration in order to get preliminary human-in-the-loop performance data from lunar exploration field trial that provides knowledge to further enhance the habitat’s capabilities for forward designs [8]. Concerning the design of the lunar outpost, the need to avoid ‘over-design’ is correctly proposed in [9], where the usual ‘aerospace approach’ to design is criticised if applied for

a stable and fixed facility with mixed uses and multiple stakeholders.

The present paper describes the outcome of a feasibility study which has been funded in 2009 by the European Space Agency (ESA) in order to explore the possibility to build structures on the Moon by using the local material. This General Study Programme (GSP) contract, entitled ‘3D printed building blocks using lunar soil’, aimed at assessing the concept of using 3D printing technology as a potential means of building habitat on the Moon. The basic idea behind this project lies in the adoption of a 3D printer of large dimension to manufacture a representative structure composed of a base material whose chemical and granular composition is very close to the ones which characterise the lunar soil, named regolith according to the definition given by Merrill in 1897 [10]. Some preliminary results of this study have been discussed in [11]; this paper, which follows the project conclusions, provides a more complete overview of the project outcomes and outlines the main results and ideas for future developments.

2. Outpost design

2.1. Outpost design requirements

The design of a Lunar outpost is one of the most fascinating challenges for architects [12]. The design of a suitable habitation for colonising the Moon requires – as a preliminary step – the definition of basic requirements representative of a credible Moon scenario, and of suitable boundaries and constraints to be respected. The definition of such requirements takes into consideration the Lunar environment and a possible mission approach.

In order to simplify the outpost design, it would be useful to decouple the task of keeping an atmosphere into the outpost from the thermal, mechanical and radiation protection functions. From this starting point, a solution has been elaborated which implies an inner inflatable module, which provides the pressurised shell for the breathable environment of the habitat, and the outer part of the outpost being ‘printed’ with Moon regolith by the D-shape system. The shell must protect the habitat from micrometeoroids and radiations; therefore the walls must be thick enough, which also provide suitable thermal insulation and capacitance. In addition, internal pressure would create strong tensile stresses in a concrete-like structure which is intrinsically fragile: removing pressure from the internal wall of the shell reduces the loads, and therefore the amount of material to be consolidated, ultimately reducing the amount of binding liquid.

The location of the outpost on the surface of the Moon must be defined by taking into account the basic reasonable environmental requirements: therefore a location close to the Moon south pole is envisaged, in order to ensure the availability of a water source, and such location should be on an elevated position (e.g. the border of a crater). This latter choice allows optimal sun exposure, as the location is sunlit almost all the time, with the sun revolving very close to the horizon with an elevation of about $\pm 1.5^\circ$, which is fundamental as the outposts should

derive a significant part of the electrical power from solar arrays [13].

The main purpose of the regolith external shelter consists in protecting the crew (and also the equipment) from radiation (by keeping the total dose over a typical six months to one year mission within a reasonable level) and micrometeoroids (chance of no penetration of 99% over a mission lifetime of 10 yr). These requirements can be achieved through a wall thickness between 1 and 2 m (depending on orientation and margins). Such a size also provides an adequate thermal insulation and a large thermal capacitance of the shield.

In terms of structural loads, three main contributors have been identified:

- Gravity.
- Moonquakes.
- Thermo-elastic loads.

The former two factors have a much lower effect with respect to the corresponding ones on Earth; however the structure is envisaged as a very thin network of consolidated material sustaining the whole mass of a 2 m-wide regolith wall. As far as the thermo-elastic loads are concerned, the presence of the Sun, slowly rotating about the outpost in about 29 days, is foreseen to produce a gradient between the sunlit and the shadow-exposed parts of the shield as well as between the internal and the external sides of the wall. The relationship between the coefficient of thermal expansion and the mechanical strength of the consolidated regolith ultimately affects the ratio between the solid and the powder.

Finally, constraints on the internal volume allocation have been derived through an extrapolation from International Space Station (ISS) experience.

The building approach has been defined by taking into account the relatively long time available for the construction: the adopted 3D printing technology allows construction scale manufacturing, but this would require to transport (and/or eventually partially mount or construct) a huge printer on the Moon. A more economic and efficient solution might consist in adopting a smaller 3D printer (1–2 m printing width) equipped with wheels (or legs), supported by another rover performing the function of collecting and laying down the regolith, such as in the example depicted in Fig. 1. The same support rover or another specialised autonomous or remotely-controlled vehicle can remove the unwanted sand from around and inside of the structures. In particular, in the exemplar case that is depicted in Fig. 1, the 3D printer should print the building blocks just around the inflatable structure that is described in the following paragraph, by thus also minimising the required movements of the blocks and the energy consumptions of the vehicles, as a consequence. This is just a possible scenario: the removal of surrounding sand is one of the problems related to the spatialization of the 3D printer which were beyond the scope of the described research work. The project mostly aimed at demonstrating that the selected 3D printing technology is physically applicable on the Moon to build a structure that has been designed to be compatible with the harsh environmental conditions that can be found there. Many other issues will surely need to be faced to plan the first space mission for building the first human outpost on the Moon.

The possibility to achieve a suitable trade-off between digging and collecting regolith from the surface could also be investigated. For instance, part of the outpost could be underground and the dug regolith could be used for construction of the cover above the surface. The purpose of

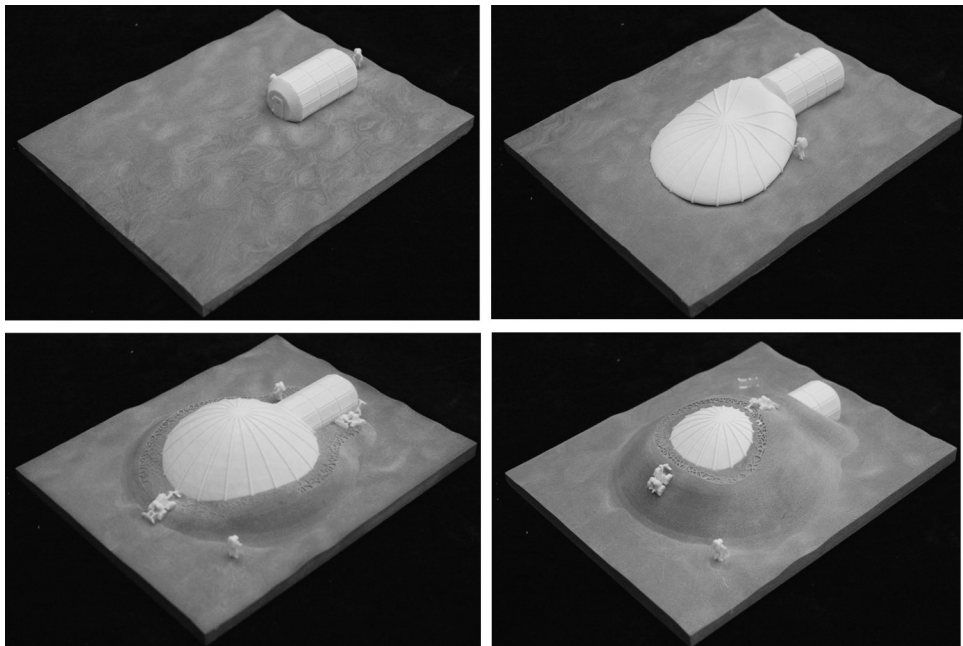


Fig. 1. Exemplar sequence of construction of the lunar outpost by means of two cooperating autonomous vehicles.

the present study has been limited to the assessment of the kind of internal structure necessary to provide the wall with a suitable resistance and stability as well as of the ratio between binder and base material (that defines the total mass of construction material to be brought from Earth).

2.2. Design and optimisation

As already underlined in the previous section, the first layer of the outpost is constituted by an inflatable pressurised structure such as the one depicted in Fig. 2. This structure could have a height of 5 m, so that it can contain two levels. The overall dimension could be in the region of 10 m × 5 m in section. The precise dimensioning of the module is beyond the scope of the present work but is investigated in ongoing work; in fact currently ESA is testing the radiation shielding capabilities of the material used within their study [14]. This concept agrees with most of potential scenarios that are currently under consideration, where fully furnished modules are supposed to be brought to the moon. To this aim, NASA organised the

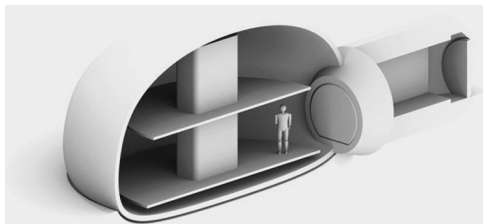


Fig. 2. Cutaway axonometry of an inflatable non-rigid structure with two levels.

X-Hab challenge for universities to propose habitats [15]. Some alternatives to build on the spot are also proposed but have not been considered here. The overall shape of this inflatable should have continuous curvature in order to most effectively withstand the internal pressures.

The overall structure of the outpost has been designed also by trying to minimise the overall amount of regolith to displace. These results can be achieved through an intermediate (temporary) inflatable element made of tubes, which is the reference for the internal wall boundary (see Fig. 3).

The tubular element can be deflated once the wall is set and reused for another module. Although this study will focus on the design of a single module, several modules could be constructed and interconnected, such as in the example depicted in Fig. 4a, according also to the concept of ‘design to evolve’ that is presented in [3] promoting a not programmatic and flexible strategy towards the first settlements on the Moon.

The wall thickness and shape have been analysed and designed as a function of the following main requirements:

- The need to keep the structure within the angle of repose [16] of the regolith, namely the maximum angle that ensures the stability of the deposited material (i.e. within which the regolith sand do not slope under the effect of the Lunar gravity), which is estimated to be equal to 40°.
- Protection from micrometeoroids, which implies an almost evenly spread minimum thickness.
- Protection from solar radiation, namely the wall must be thicker in the directions facing the Sun, as a greater part of radiation is associated to solar flux. An example of possible exposure to solar radiation of a group of different habitation modules is depicted in Fig. 4b.

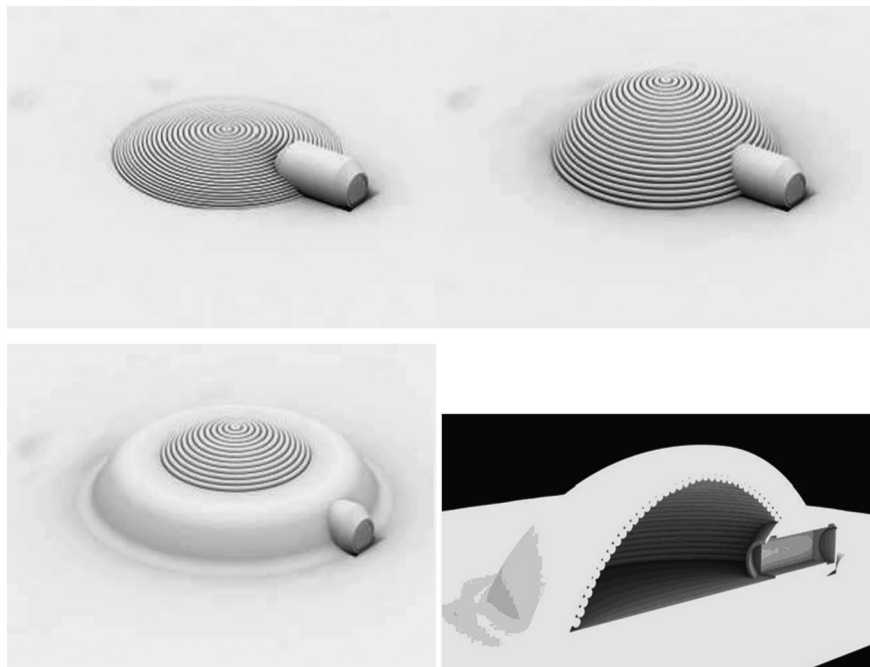


Fig. 3. Example of wall construction sequence through an intermediate temporary inflatable support composed by tubes.

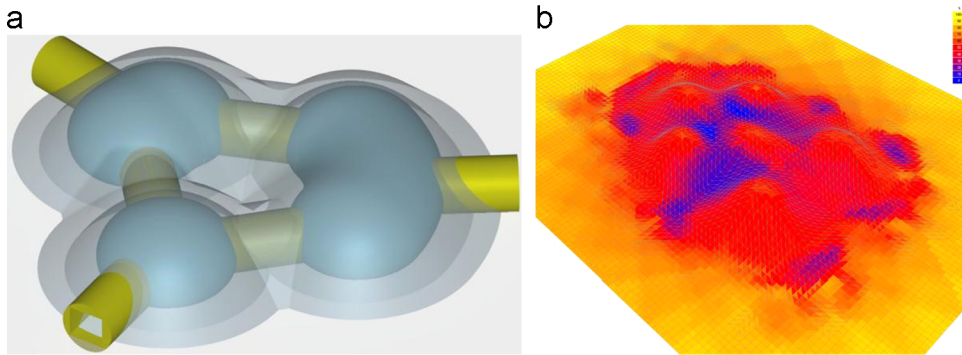


Fig. 4. (a) Example of a combination of several habitation modules; (b) corresponding percentage exposure of modules to solar radiation.

For the internal profile of the wall a catenary arc has been selected. A catenary is the ideal shape for a freestanding arch of constant thickness. The catenary is the curve that an idealised hanging chain or cables assumes when it is supported at its ends and acted only by its own weight [17]. There are many examples in architecture of hanging chains models used to calculate the optimum form of structures; the Colonia Guell Church was developed by Gaudi by exploiting the hanging model. Such model is based on the theory of 'reversion of the catenary', for which only tension forces can exist in the chain. The form of the catenary upside down gives a perfect shape for an arch of stone masonry, in which only reversed forces of tension, being compression, occur. As the 3D printed regolith, such as mansory, has a very low tensile strength, the geometry of the structure ensures that forces are primary compression. The catenary structure has been selected for the outpost internal profile in order to span the internal pressurised volume in a way that ensures that mostly compression forces act on the structure itself.

Due to the virtual absence of atmosphere and magnetic field, space radiation on the Moon is far higher than on Earth: actually three types of radiation reach the Moon surface: solar wind, solar flares and Galactic Cosmic Rays (GCR). In order to protect the inner core of the outpost from radiations, a regolith cover of 1500 mm must be located in the direction of the sun rays. Moreover the geometry and the catenary curve can be horizontally offset by 1500, in order to ensure the required protection against the solar radiation.

Finally meteorites must be considered, which impact on the moon at speed values close to 18 km/s due to the lack of atmosphere. Although large meteorites are quite rare, a sufficient protection layer for meteorite impacts is required, which is provided by a protection layer of 800 mm. Such protection is achieved by offsetting the catenary structure in the radial direction (as meteorites can impact the surface under any angle) by 800 mm. The two offsets (for protection against meteorites and radiations, respectively) in 3D create two intersecting surfaces. In order to create one overall skin, a best fitting catenary curve is draped over the two previous one. This curve does not need to be a precise catenary as it does not have any structural implication, but any point of such curve still falls within the angle of repose. The resulting line follows the angle of repose and has a tangent curve continuity so as to fit the single curve. The third offset from the catenary,

together with the offsets for meteorite and radiation protection, gives the shell thickness, which is calculated to support the necessary addition of regolith and additional loads.

The final structure has a variable thickness over its cross section: thickness is greater at the rim, where it meets the horizontal ground plane, and thinner at the zenith. **Fig. 5** depicts in a schematic way the outpost structure with all its superimposed layers.

The structural design work has been focused on the optimisation of the internal elements of the wall structure in order to minimise the ratio between consolidated material and rough regolith. The result of such trade-off is provided by a particular topology named closed foam (see **Fig. 6a**). Closed foam structures are defined as foam patterns with fully enclosed bubbles without interconnected pores. Normally the closed cell foams have higher compressive strength than open foams: in fact, cell faces, which act as plates, reduce bending forces at nodes. This has advantages when considering meteorite impact, but also with respect to general robustness. Closed foams offer perceived advantages due to compartmentalisation of loose regolith within the structure. This means that any piercing of the shell would not lead to a leaking of unglued regolith which might be the case in open cell foam. The loose regolith is kept into the bubbles and becomes part of the outer shell, by contributing to protect the inner core despite of not being aggregated. Thus the closed foam structure also minimises the need for binding material: in fact approximately 10% of the sand that constitutes the outer shell must be actually dried with the binding liquid. **Fig. 6b** depicts an exemplar structural element that has been practically manufactured in the project, as described in **Section 7**.

2.3. Structural feasibility study

A structural feasibility study has been pursued making some simplifying assumptions and by performing a structural analysis on a shell structure, a comparative Finite Elements (FE) structural analysis on small samples with different cell sizes and an analytical study comparing the cell structure with other materials.

To start to understand the structural requirements for the dome, the assumption has been made that only the inner side of the dome has a structural performance. Another major assumption consists in the fact that the support conditions for

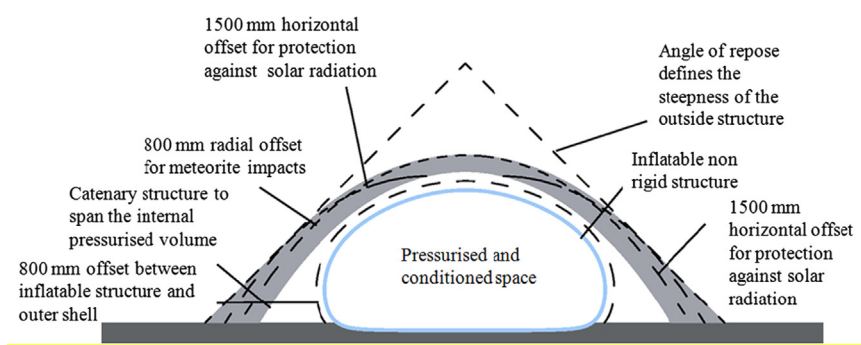


Fig. 5. Schematic description of the outpost structure.

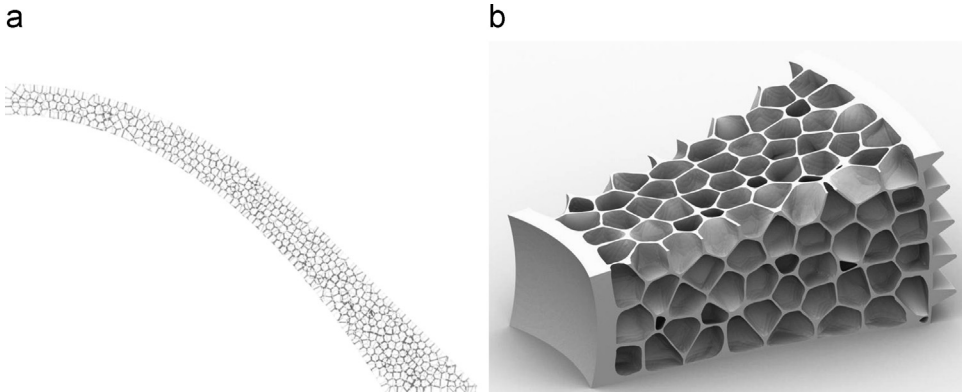


Fig. 6. (a) Wall profile; (b) exemplar structural element.

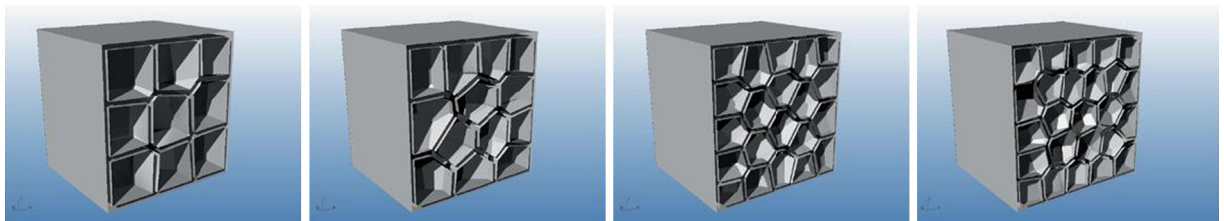


Fig. 7. Four examples of the tested block with different cell sizes (courtesy of Fosters+Partners)

the dome should be such that vertical restraint is provided to the edge of the dome, but no resistance is present in the horizontal direction, namely the shell can 'slide' outwards under the effect of its own weight. This is obviously an extreme case, since it should be possible to dig the foundations in a way that some horizontal support is also provided. Under these assumptions, if the composite shell thickness can be reduced to a value of the order of 130–150 mm, i.e. at this thickness the size of the tensile stress due to the boundary conditions is within a nominal allowable tensile stress. This simple feasibility study suggests that, in principle, one can build the dome using a thin inner shell of composite material covered by the required thickness of non-compacted regolith.

However, one must be sure that the non-compacted regolith is not removed by external agents and this was the main reason behind the choice of a more complex cellular structure keeping the regolith attached to the shell but not requiring an excessive amount of binding material, namely

the closed foam structure described in Section 2.2. Digital models of five different variations of cell size (see four of them in Fig. 7) for a regolith-based foam cube with a side of 500 mm were analysed with the FE analysis software Scan&Solve™ to assess its effect on structural strength.

The relative density was kept constant across these tests by adjusting the wall thickness, so that each block has the same mass of solid material. A 10 kN load has been applied to the top face of the cube, with the bottom face restrained. The results have been compared in terms of maximum Von Mises stress: Table 1 depicts the results of such analysis for the four blocks depicted in Fig. 7. This investigation allowed to find the optimal dimension of the bubbles of the closed foam for the final demonstrator.

Considering the fact that the properties of cellular solids are often directly proportional to their relative density, the impact of this factor on the stiffness has also been evaluated, as on the Moon only a finer amount of

Table 1

Maximum Von Mises stress and main features of the 4 foam blocks in regolith depicted in Fig. 7.

Average cell size (mm)	Wall thickness (mm)	No. of cells	Max Von Mises Stress (MPa)
190	24	50	0.35
150	19.8	100	0.28
130	17.3	150	0.28
103	15.2	250	0.23

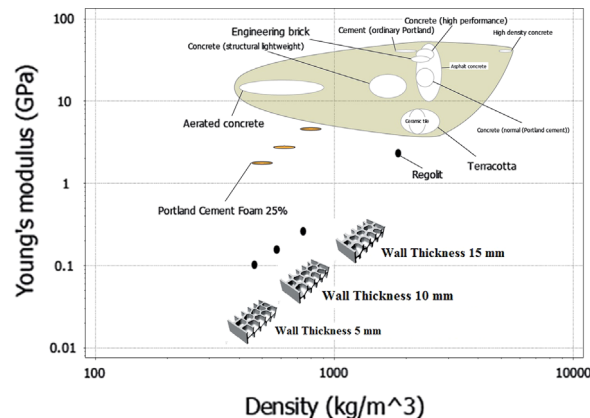


Fig. 8. Stiffness vs. density diagram of 3 exemplar regolith foam blocks.

binder will be available and is therefore fundamental to understand how best to distribute the material in the dome shell volume. Analytical models described by Gibson and Ashby [18] have been used to estimate the change in mechanical properties with relative density. The results have been compared on 'Ashby Plots' with other cementitious materials, solid and cellular. The diagram depicted in Fig. 8 provides the example of such comparative analysis, as it shows the predicted stiffness of 3 exemplar regolith foam blocks characterised by different values of the wall thickness and, thus, different relative densities.

A similar simulation-based analysis has been pursued for other relevant properties, such as compressive and flexural strength, and this provided useful indications for final the design of the walls and of the demonstrators that have been finally produced during the printing tests, whose results are described in Section 6.

3. The regolith simulant

In order to perform the experiments on the construction of building blocks, a material needed to be found, which was as similar as possible to the Lunar soil. Therefore a deep study has been pursued in order to select an adequate and affordable regolith simulant, by considering its chemical and physical properties, main chemical elements and compounds, respectively, of the lunar soil.

As far as the chemistry is concerned, the simulant must be representative of the lunar soil with respect to the chemical compounds playing a role in the chemical reactions at the base of the reticulation process. Tables 2 and 3 report the contents of the main chemical elements and compounds of the lunar soil, respectively [19]. The binding

Table 2

Contents of the main chemical elements of the Lunar soil compared to average Earth soil composition.

Element	Lunar highland	Lunar Maria	Earth
Oxygen	44.636	41.400	46.885
Silicon	21.017	21.048	27.869
Aluminium	13.311	6.920	8.180
Iron	4.874	13.105	5.031
Calcium	10.689	7.823	3.652
Sodium	0.310	0.288	2.847
Potassium	0.080	0.109	2.606
Magnesium	4.554	5.719	2.103
Titanium	0.310	3.078	0.443
Hydrogen	0.006	0.005	0.141
Phosphorus	0.050	0.066	0.106
Manganese	0.068	0.169	0.096
Carbon	0.010	0.010	0.020
Chlorine	0.002	0.003	0.013
Chromium	0.085	0.258	0.010

ink interacts with the metallic oxides that are a natural component of regolith, enabling a crystallisation process which envelopes and links the small grains of the regolith powder. While in lunar regolith these metal oxides are available in free form, on terrestrial simulants they are usually in the more inert form of hydrated compounds. For this reason, the regolith simulants have typically to be doped with some metal oxides in anhydrous condition.

Among the physical properties, the most important one is granulometry, as the process quality and the mechanical properties of the consolidated product are influenced by grain size. Table 4 reports the granulometry of the lunar soil [19]. Granulometry plays an even more important role during vacuum reticulation (that is explained in Section 4). It is therefore of utmost importance that granulometry of the simulant is representative of lunar regolith.

The cost factor needed to be considered as well, due to the need to manufacture a building block of sufficiently large size. Since the purpose of such demonstration is to show the level of construction complexity that is achievable through the D-shape 3D printing technology, the resolution cannot be scaled down and a 1:1 scale section of the wall has been chosen. To have a portion which is large enough to show the features of the printed item, about a cubic metre of regolith simulant was needed, thus the mass of simulant to be purchased lies between 2 and 3 metric tonnes. Table 5 summarises the most commonly referred simulants of the lunar soil.

The cost of this amount of commercial lunar soil simulants (e.g. JSC-1A from Orbitec of Madison, WI, USA or CAS-1 from the Chinese Academy of Sciences) is of about 40–50 k€, which was not affordable within the project. Therefore, an alternative simulant source has been established and its characteristics have been compared to JSC-1A, which has been chosen as reference since it is promptly available and therefore widely adopted. Moreover both regolith simulants have been compared to the actual lunar regolith.

The newly developed regolith simulant has been named DNA and is based on a natural volcanic material, that can be found close to the Bolsena Lake (Italy).

The results of the chemical analyses, (the oxide contents are reported in Table 6) show that the composition of

Table 3

Contents of the main chemical compounds of the Lunar soil.

Mineral	Dana #	Mohs hardness	Spec. gravity	Chemical composition	% ^a
Plagioclase					
Anorthite	76.1.3.6	6	2.75	$\text{CaAl}_2\text{Si}_2\text{O}_8$	A
Bytownite	76.1.3.5	6.0–6.5	2.73	$(\text{Ca},\text{Na})(\text{Si},\text{Al})_4\text{O}_8$	M
Labradorite	76.1.3.4	7	2.71	$(\text{Ca},\text{Na})(\text{Si},\text{Al})_4\text{O}_8$	M
Olivine					
Fayalite	51.3.1.1	6.5–7.0	4.39	Fe_2SiO_4	m
Forsterite	51.3.1.2	6.5–7.0	3.24	Mg_2SiO_4	M
Pyroxene					
Clinoenstatite	65.1.1.1	5.0–6.0	3.4	$\text{Mg}_2[\text{Si}_2\text{O}_6]$	M
Pigeonite	65.1.1.4	6	3.3	$(\text{Mg},\text{Fe}^{+2},\text{Ca})_2[\text{Si}_2\text{O}_6]$	M
Hedbergite	65.1.3a.2	6	3.4	$\text{CaFe}^{+2}[\text{Si}_2\text{O}_6]$	m
Augite	65.1.3a.3	5.5–6.0	3.3	$(\text{Ca},\text{Na})(\text{Mg},\text{Fe},\text{Al},\text{Ti})(\text{Si},\text{Al})_2\text{O}_6$	M
Enstatite	65.1.2.1	5.0–6.0	3.4	$\text{Mg}_2[\text{Si}_2\text{O}_6]$	A
O					
Ilmenite	4.3.5.1	5.5	4.72	$\text{Fe}^{+2}\text{TiO}_3$	m
Spinel					
Spinel	7.2.1.1	7.5–8.0	3.56	MgAl_2O_4	m
Hercynite	7.2.1.3	7.5–8.0	3.93	$\text{Fe}^{+2}\text{Al}_2\text{O}_4$	m
Ulvospinel	7.2.5.2	5.5–6.0	4.7	$\text{TiFe}^{+2}\text{Al}_2\text{O}_4$	m
Chromite	7.2.3.3	5.5	4.7	$\text{Fe}^{+2}\text{Cr}_2\text{O}_4$	m
S					
Troilite	2.8.9.1	4	4.75	FeS	t
PO ₄					
Whitlockite	38.3.4.1	5	3.12	$\text{Ca}_9(\text{Mg},\text{Fe}^{+2})(\text{PO}_4)_6(\text{PO}_3\text{OH})$	t
Apatite	41.8.1.0	5	3.19	$\text{Ca}_9(\text{PO}_4)_3(\text{OH},\text{F},\text{Cl})$	t
Native iron	2.9.1.1	4.5	7.87	Fe	t

^a Typical relative abundance, A-abundant, M-major, m-minor, t-trace**Table 4**
Granulometry of the Lunar soil.

Grain size (mm)	% Weight
10–4	1.67
4–2	2.39
2–1	3.20
1–0.5	4.01
0.5–0.25	7.72
0.25–0.15	8.23
0.15–0.090	11.51
0.090–0.075	4.01
0.075–0.045	12.40
0.045–0.020	18.02
less than 0.020	26.85

the new simulant is at least as close as that of JSC-1A to the composition of real regolith. The main difference between the two simulants and lunar soil is in the oxidation state of iron, which is mainly trivalent on the Earth while it is bivalent on the Moon. From the point of view of the 3D printing process which is considered here, it is also very relevant that the real lunar soil contains a higher amount of MgO, which is required as one of the reactants that allows the printing process to occur.

Crystallographic analysis through X-Ray Diffraction (XRD) and optical microscopy has also been pursued in order to find the major mineral species in DNA regolith samples. This analysis put into evidence the following major crystalline phases, listed in order of abundance in Table 7.

Such analysis shows that the similarity of DNA-1 to lunar samples is not worse than that of JSC-1A, although no olivine has been found. Analcime or analcite (from a Greek word which means 'weak' due to the poor capability of this ore to charge energy after being rubbed) is a white, grey, or colourless tectosilicate mineral. Analcime consists of hydrated sodium aluminium silicate in cubic crystalline form and its chemical formula is $\text{NaAlSi}_2\text{O}_6 \cdot \text{H}_2\text{O}$. In a small percentage of cases, potassium or calcium substitute sodium exists. A silver-bearing synthetic variety also exists (Ag-analcite). Analcime is usually classified as a zeolite mineral, but structurally and chemically it is more similar to the feldspathoids. Analcime occurs as a primary mineral in analcime basalt and other alkaline igneous rocks. It also occurs as cavity and vesicle fillings associated with prehnite, calcite, and zeolites.

By milling, sieving, and remixing, the required granulometry can be easily achieved as well.

4. Manufacture of the building blocks

4.1. Direct manufacturing techniques

Direct Manufacturing techniques derive from the Rapid Prototyping systems developed in Japan and USA during the late 1980's and 90' [20] and consist of an additive process which constructs three dimensional objects through the automated curing and/or deposition of successive layers of material. There is a wide range of direct manufacturing machines commonly called '3D Printers' which use different additive processes and materials and are applied for a many

Table 5

Summary of the most common regolith simulants.

Source: NASA, <http://isru.msfc.nasa.gov/lib/Documents/Simulant-listing.pdf>.

Simulant	Info	Type	Contact info
United States:			
ASL	Arizona Lunar Simulant Desal et al., 1993	Low-Ti Mare (geotechnical)	
BP-1	KSC/Arizona Black Point quarry waste (Basalt); using for large scale excavation exercise with BLADE Rahamation and Metzger, in press	Low-Ti Mare (geotechnical)	Rob Mueller/KSC
CSM-CL	Colorado School of Mines - Colorado Lava Unpublished	Geotechnical	
GCA-1	Goddard Space centre Taylor et al. 2008	Low-Ti Mare (geotechnical)	
GRC-1 & -3	Glenn Research Centre (Sand, clay mixture used in SLOPE Facility for mobility/excavation) Oravec et al., in press	Geotechnical: standard vehicle mobility lunar simulant	Allen Wilkinson/GRC
GSC-1	Goddard 'simulant'; material from local site that is being used for drilling tests		Peter Chen/GSFC
JSC-1*	Johnson Space Centre McKay et al., 1994	Low-Ti Mare (general use)	No longer available
JSC-1A, -1AF, -1AC	Orbitec created under a NASA contract	Low-Ti Mare (general use) (JSC-1A was produced from the same source material after a gap of some years when JSC-1 ran out)	http://orbitec.com/store/simulant.html
MSK-1	Carpenter, 2005	Low-Ti Mare (intended use unknown)	
MSL-1*	Minnesota Lunar simulant Weiblein et al., 1990	High-ilmenite mare (general use)	No longer available (created in the 1980s)
MSL-1P*	Weiblein et al., 1990	High-Ti Mare (experimental, not produced in bulk although small quantities were distributed)	
MSL-2*	Tucker et al., 1992	Highlands (general use)	
NU-LHT -1M, -2M, -1D, -2C	NASA/USGS highland type simulant (chemical/mineralogical & physical properties) Stoeser et al., 2009	Highlands (general use)	Carole McLemore 256-544-2314 Carole.A.McLemore@nasa.gov http://isru.msfc.nasa.gov
Others			

Table 6

Comparison of the contents of the main oxides of JSC-1A, DNA, and an average of lunar soil samples from Apollo missions [20].

Oxide	DNA-1	JSC-1A	Lunar soil 14163 (mean of the Apollo missions)
Unit	(Wt%)	(Wt%)	(Wt%)
SiO ₂	41.9	41	47.3
TiO ₂	1.31	1.6	1.6
Al ₂ O ₃	16.02	15.9	17.8
Fe ₂ O ₃	14.6	18.1	0.0
FeO	0.00	0.00	10.5
MgO	6.34	4.73	9.6
CaO	12.9	13.2	11.4
Na ₂ O	2.66	2.5	0.7
K ₂ O	2.53	1.05	0.6
MnO	0.213	0.24	0.1
Cr ₂ O ₃	0.00	0.03	0.2
P ₂ O ₅	0.341	0.63	0.00
LOI	0	0.00	0.00
Total	98.9	99.0	99.8

different purposes [21–23]. More properly, the matter of direct 3D printing of buildings or building blocks falls into the general field of Construction or Full Scale Manufacturing Methods [24–26].

These methods are now maturing. Current technologies are now being scaled up for the manufacture of full-size components and systems; these can be defined to neatly fit into three categories: Metal, Polymers and Synthetic stone. A number of construction and full scale manufacturing techniques have been developed since the mid 90's. These include Solid Freeform construction [27], Robocrane [28,29], Additive Plaster (Bert Brink, Maxit group), Freeform Construction [30] developed at the Rapid Manufacturing Research Group in Loughborough, Contour Crafting [31,32] and the Monolite machine [33], which a few years later evolved into the D-shape technology. The first three techniques presently are not actively pursued, while Contour Crafting, Monolite/D-shape and Freeform Construction machines are under continuous development and are currently used to produce walls and large sculptural objects. In particular, D-shape with respect to the other techniques proved to be very effective in printing very large scale objects: for instance, it allowed to build in one single printing process a whole house, which is depicted in Fig. 9.

Each of the three above cited techniques exploits slightly different deposition methods, processes and materials. The greatest difference among these techniques of them [27,32] selectively catalyses materials within a layer of pre-deposited substrate, while the remaining ones

Table 7

Comparison of the major crystalline phases of JSC-1A, DNA, both listed in order of abundance.

DNA-1 major crystalline phases	JSC-1A major crystalline phases
Analcime (Feldspatoid mineral)	Plagioclase (Feldspar mineral)
Pyroxene (Diopside)	Pyroxene (Diopside)
Mica (phlogopite)	–
–	Olivine (Forsterite)
Traces of Calcite	Calcite
Traces of Quartz (Silicon dioxide)	Traces of philllosilicate (micas, serpentine talc, clay minerals)



Fig. 9. A complete house printed in one single process through the D-shape technology. [34]

exploit a technique which extrudes building materials premixed with a binder or catalyst, which are thus similar to concrete.

In particular, the Freeform Construction machine is in principle similar to Fused Deposition Modelling (FDM) additive manufacturing systems [35]. This system is designed to extrude and deposit material at multiple layer resolutions within the same build, above and below 6 mm and its development is presently focusing on creating complex panels (i.e., ‘building blocks’), rather than entire buildings. The particular benefit of this system when it will be fully operational should be the broad range of materials that could be used, including support material. On the other hand, the Contour Crafting machine extrudes two thin parallel layers of material, leaves the inner surfaces unfinished and the outer surfaces are robotically finished with a trowel mounted on the printing head. The space between the two layers can then be filled with sand or other materials. This technique has been proposed to NASA as ISRU technology for Moon buildings [32].

4.2. The D-shape technology

In the present work, the patented D-shape technology, has been exploited, which is a three-dimensional printing system for producing conglomerate building or building blocks according to two different methods invented and patented by the Italian engineer Enrico Dini. The first ‘printing’ method

allows to produce directly on site the entire building structure, while the second method is conceived to print ‘off site’ – or better ‘beside site’ – a set of building blocks to be assembled together, eventually using additional reinforcements. The printing machine is a sort of gigantic plotter, with a spraying head which moves along two frames in the x-y axis space and selectively sprays on predefined areas of the sand layer a binding liquid also indicated in the following as ‘ink’. A set of four stepper motors move the frame on the z-axis. A schematic view of the apparatus is given in Fig. 10a, while Fig. 10b depicts the complete apparatus.

The core of the system is the ‘printing head’, which act also as solid material spreader at the beginning of the printing process (see Fig. 11).

The solid material spreader/printing head is mounted on a 6 m aluminium beam which can span horizontally the printing area, and moves according the prefixed vertical pitch. The printing head is composed of 300 nozzles at 20 mm inter-axis distance, thus covering the 6 m printing advancing front. To fill the 20 mm gap within the nozzles, and to ensure that the whole area to be printed would be uniformly reached by the liquid ink, the printing head shifts along a y auxiliary axis. This perpendicular movement is ensured by an AC electric piston controlled in position by an incremental encoder having 0.5 mm positioning accuracy. The head holds the hydraulic piping and wiring that provide feeding the nozzles, and two peripheral control units linked to the CPU via profibus cable. The gantry holding the printing head is internally void and is cyclically filled with the granular material which is then deposited to form the next ‘layer’. The ‘sand’ is strained in a thin layer by a shaving blade during the beam movement along its main x axis. A set of rolling cylinders provide an homogeneous sand pressure prior to start printing on the newly deposited layer. A gear motor and an encoder ensure a 1 mm positioning accuracy.

Nozzles are activated by a 2-ways microvalve, operated by a 24 Volt DC ON/OFF servo driven solenoid operated in pulsed mode to regularly jet drops of preset volume. Valve on/off response time is in the order of 10–15 ms. Fig. 12a depicts the details of the nozzle; in particular some details are highlighted, which are:

1. Valve body.
2. O ring.
3. Head gasket.
4. Thrust spring of the coil body.
5. Rear stop of the piston.
6. Solenoid coil.
7. Gasket.

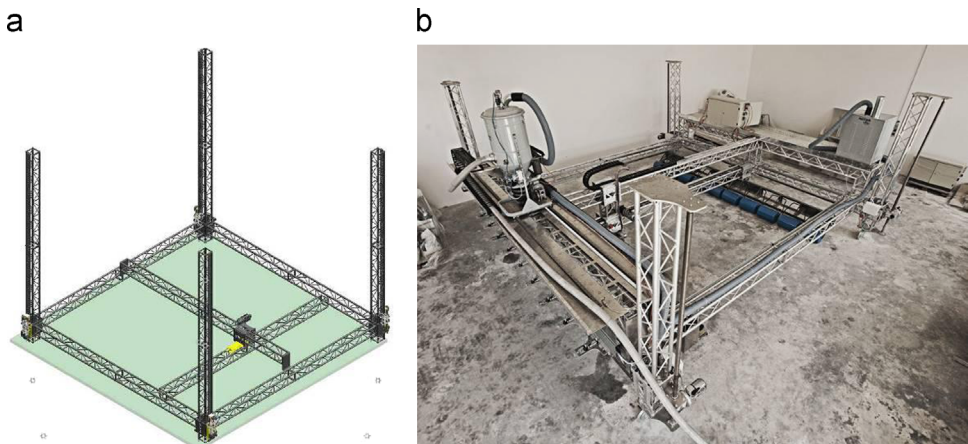


Fig. 10. (a) Schematic of the D-shape Material Depositing Unit and (b) the complete D-shape printer.

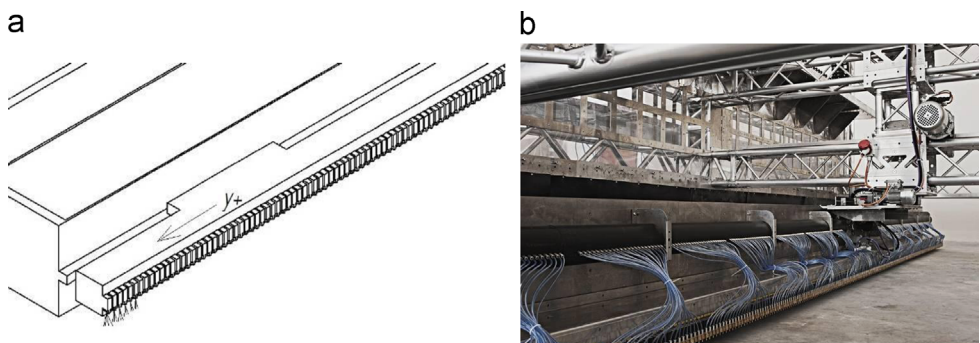


Fig. 11. (a) Schematic of the mobile depositing unit holding a set of spraying nozzles and (b) the printing head of D-shape 6×6 model with 300 nozzles.

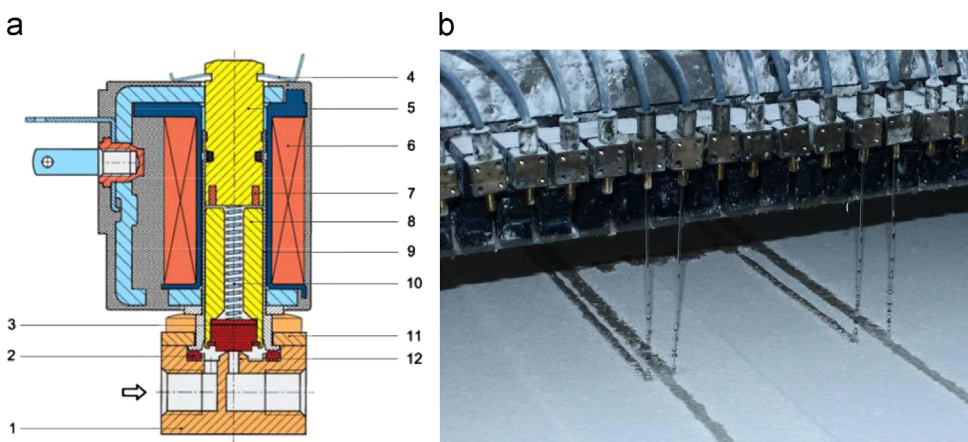


Fig. 12. (a) Detail of a single binder deposition device and (b) detail of the printing process, where the binder is sprayed on the sand.

8. Piston in soft iron (i.e. the piston is not permanent magnetic).
9. Brass cylindrical case.
10. Closing spring.
11. Valve cover.
12. Feeding channel for the binding material.

The working range of temperature is from -10°C to $+60^{\circ}\text{C}$. Fig. 12b provides a detailed view of the deposition process.

The 'Ink' flow rate depends on nozzle upstream pressure and on nozzle shape. The link between the flow rate Q (in m^3/h), the hydraulic pressure drop Δp (expressed in mmH_2O) and the flow constant K_v is expressed by the following formula:

$$Q = K_v \sqrt{\frac{\Delta p}{10}} \quad (1)$$

Taking into account the advancement speed of the printing head (10–20 cm/s), the stoichiometry of the reaction, the

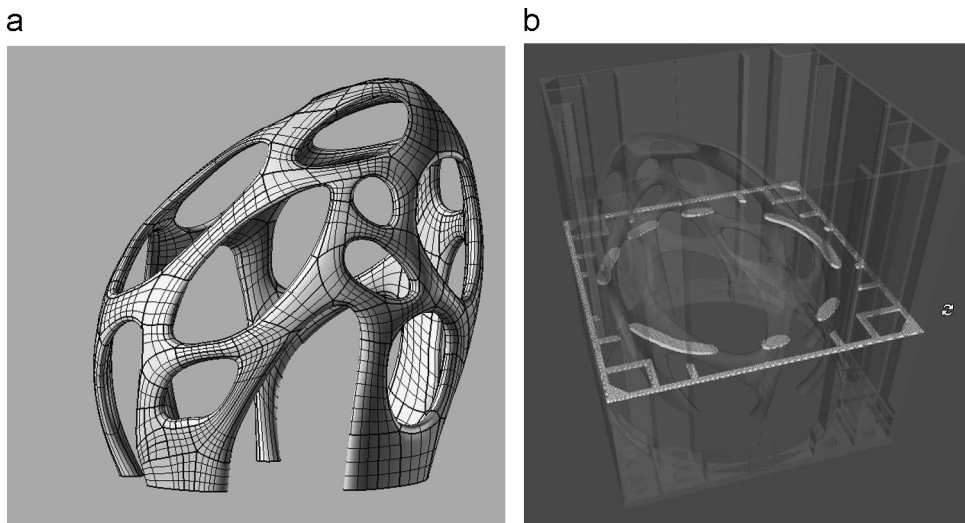


Fig. 13. (a) A 3D model of the building structure and (b) an exemplar model cross section with its containing shell.

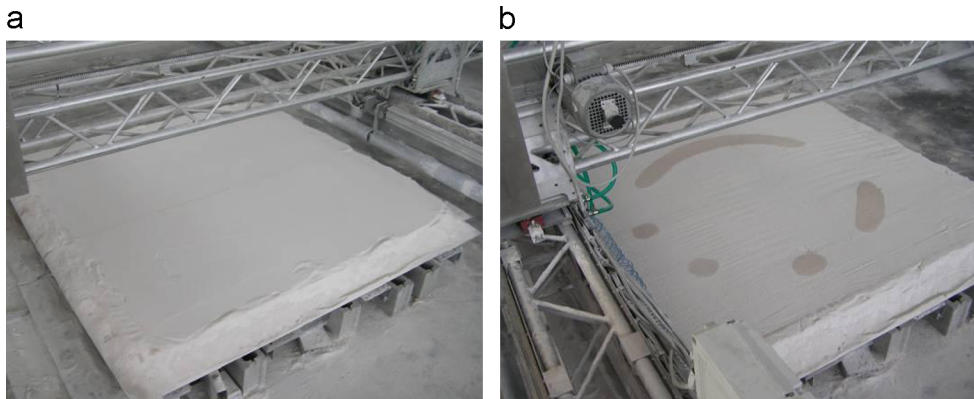


Fig. 14. (a) A layer of deposited granular material and (b) a cross section of the model which has just been printed.

thickness and granulometry of the sand layer, and finally the hydraulic pressure drop, a suitable flow rate is imposed. The volume of the drop released by the nozzle is also related to the viscosity of the liquid (max allowed 22 c Stokes). Each nozzle is independently fed to ensure a reliable flow rate.

4.3. The printing procedure

The D-shape technology has been originally conceived to build medium-size structures in a one shot process. The building procedure consists of the following steps:

- (1) Modelling of the structure model embodied in a containing shell with a 3D CAD software. As an example, Fig. 13a, depicts a small-scale model (2 m height) of an artistic structure called 'Radiolaria', which has been built with the D-shape machine.
- (2) The 3D model has then to be 'dissected', by using horizontal planes (or sections) with a regular pitch (see Fig. 13b, where the pitch is set to 5 mm). The obtained 2D plans are sequentially sent to the machine in bottom-up order.

(3) Printing the structure according to the following sub-steps:

- (3.1) A uniform horizontal layer of granular material of thickness corresponding to the prefixed pitch (e.g. 5 mm) is deposited by the machine (see Fig. 14a); the granular material has to be preliminarily mixed with pulverised metal oxide which reacts later with the binding liquid.
- (3.2) The mobile spraying heads move horizontally and a predetermined amount of liquid is sprayed on those parts of the layer which has to be bound (such as depicted in Fig. 14b). A chemical reaction between the metal oxide and the liquid salt takes place and parts of the building are 'printed'. The distance between the nozzles is equal to 20 mm, while the average drop diameter is 5 mm wide. Therefore the layer cannot be completed in one single printing session. To fill the gap (which is clearly visible in Fig. 12b) between the nozzles an additional movement must be added, which shifts the printing head aside along the y-axis, so that the mobile head can print the bitmap of the considered layer in 4

subsequent strokes all performed at the same value of the z coordinate.

- (3.3) The horizontal frame is lifted up of the prefixed pitch on the z-axis; a second uniform layer of granular material is then laid on the first one and, at the same time, the layers are pressed by the machine with a pressure which can be set from 0.05 kg/cm² to 0.5 kg/cm².
- (3.4) Point 3.2 is repeated with new spraying coordinates.
- (3.5) Points 3.2–3.5 are repeated the required number of times, until the model is completed.
- (4) At the end of the process, the containment shell has to be removed in order to expose the building structure.

The D-shape machine can be used to print ‘blocks’ instead of ‘buildings’ and this is the application envisaged to build the lunar outpost.

5. Experimental demonstration of the applicability of the D-shape technology in the space

Like for any other technology which has been originally developed for terrestrial application, also the D-Shape technology is foreseen to undergo a thorough re-engineering before it can be profitably and safely applied in space. The architecture and the configuration of parts need to be redesigned to meet the mission objectives, all printer materials must be reconsidered in terms of mass efficiency, vacuum outgassing behaviour and robustness to environmental stresses. Also all the electrical, electromechanical and electronic components need to be designed and constructed according to the space standards (e.g. in terms of radiation hardness, derating, etc.). None of these issues do represent a critical showstopper for the successful validation of this technology in space; moreover the feasibility of the spatialization of such technology is beyond the scope of the present work. Here only a particular issue has been investigated, which is crucial for the application of D-Shape to the construction of building elements on the Moon using in-situ resources, namely the capability of the ink to survive and to reproduce the reticulation process in the lunar environment, i.e. in vacuum and at a representative temperature. In principle, also these features are not strictly mandatory, as one could reproduce an artificial atmosphere in the surroundings of the element being built, for the required duration (about 30 kg of water are required to fill a dome of about 2000 m³ volume at room temperature $T_R=20^\circ\text{C}$ and a pressure of 20 mbar, which is more or less the vapour pressure of the ink at that temperature). However, the demonstration that the technology can directly work in the Moon environment makes the system simpler, reduces the amount of elements, parts and mass to be brought from Earth, and, ultimately, gives it a better chance for selection. As for all chemical reactions, reticulation time increases with decreasing temperature. Conversely, evaporation increases with temperature and a trade-off must be reached between speed and mass efficiency of the printing process. Considering the importance of mass in interplanetary transportation, the trade-off will likely go towards a cold and slow process. The purpose of the present experiments was limited to show that the ink does not boil nor freeze once sprayed on the

regolith in vacuum and that it remains liquid for a time interval sufficient to let the reactions involved in the reticulation process take place. The starting point is the temperature T_R of the laboratory where the experiments have been developed.

5.1. Analysis of the boiling point

Some analysis have been performed to devise a method to avoid excess evaporation or boiling-off of the ink. Thus the ink properties in terms of vapour pressure and surface tension have been analysed. At $T=T_R$ the vapour pressure is lower than 2 kPa=20 mbar while surface tension is about 0.1 N/m. To avoid boiling and rapid vaporisation, which may eventually lead to freezing of the ink, the ink must be constrained in small volumes (e.g. drops or cavities) having an internal pressure (induced by surface tension) higher than 20 mbar. The minimum (critical) drop radius r_{cr} required to achieve the above condition has been calculated and the typical size of the cavities within lunar regolith or terrestrial regolith simulants has been evaluated. If the dimension of the cavities (at most) is smaller than $2r_{\text{cr}}$, then the behaviour of the drops of the liquid ink is driven by surface effects (capillarity) and no boiling occurs. Since the evaporation rate is limited in these conditions, heat transfer is also reduced and freezing is also prevented if the initial temperature is high enough. The pressure inside a drop of liquid in vacuum is given by the well known Young-Laplace law [36]:

$$P = 2\frac{\gamma}{r} \quad (2)$$

where P is pressure, γ is surface tension of the liquid and r is drop radius. For the values provided above, at T_R the critical radius to obtain $P > 20$ mbar is about 0.1 mm. To avoid boiling (at T_R) the size of gaps within the regolith must thus be lower than $2r_{\text{cr}}=200\text{ }\mu\text{m}$.

Radius of gaps within an array of packed spheres is always lower than that of spheres. E.g., for poorly efficient Simple Cubic Packing (SCP), radius of gap is 73% of radius of sphere. Therefore, particles smaller than $2r_{\text{cr}}$ ensure that the maximum size of water drops is lower than boiling threshold and the liquid fills the gaps by capillarity without boiling. To ensure this condition, there must be enough particles with a size smaller than $2r_{\text{cr}}$. In particular, this occurs in a packed regolith if the total volume of particles with size equal or smaller than $2r_{\text{cr}}$ is more than 48% (void/full ratio of SCP) of the total volume of construction regolith. Regolith from Apollo 11 samples is such that 73% of mass is constituted by particles smaller than 150 μm , and 81% is smaller than 250 μm , therefore regolith of this kind could be used as-is, with no need for additional milling or sieving: the printing system shall only ensure that the powder is well packed and that the ink is directly injected inside the regolith, with the ink droplets being surrounded by powder all around and without direct exposure of the ink to the external environment.

To be complete, this analysis should be extended to assess the whole functional temperature range, in order to provide in-situ operational constraints which will drive the system design and the operations schedule (e.g. with respect to periods of solar illumination). Aspects like

variation of vapour pressure and surface tension with temperature and concentration of ink components, as well as evaporation rate and freezing risk, should be taken into account. The above described calculations; however, showed that the process has a chance of success when performed in vacuum, under suitable conditions.

5.2. Vacuum tests

Tests in a vacuum chamber have also been performed in order to show that the process works and a good reticulation can be achieved in vacuum. The vacuum tests aimed at:

- Verifying the actual feasibility of the chemical process in vacuum environment.
- Analysing the behaviour of the structural ink when it is sprayed in vacuum.
- Demonstrating if the direct injection of the ink below a simulant layer can prevent the vaporisation of the fluid.
- Measuring and weighting the reticulated regolith and to compare it with the volume of injected ink.
- Qualitatively assessing the solidity of the in-vacuum reticulated compound.

The conceived protocol for ‘printing in vacuum’ basically consists in directly injecting the ink just some millimetres beneath the simulant layer, to make the regolith compactness maintain the surface tension of the ink drops so as to avoid at maximum extent all evaporation phenomena. This has been achieved by providing the final part of the ink feeding duct with a thin nozzle (2 mm of external diameter) which was inserted into the simulant as a needle (see Fig. 15a). A circular sliding dish has been designed and manufactured around the nozzle either to keep down any possible blow of the simulant due to the feeding pressure and to smooth the surface of the simulant during the displacement of the ‘printing head’. In order to perform more than one injection in the same vacuum cycle, a moving platform has been applied to move a box containing the simulant while the injector was kept fixed, approximately in the centre of the vacuum chamber. To assess the amount of ink injected in the simulant, a valve of the same type used by the D-shape printer and controlled by a PLC placed out of the vacuum chamber has been used.

The spraying valve was sustained by a supporting structure. A vertically adjustable flange allowed to place the valve at the desired height, in order to match with the surface of the regolith simulant. The simulant was contained in a suitable tray that was fixed on the moving platform operated by an external stepper motor which translated it in steps of a few centimetres, after every opening intervals of the valve. The test setup is schematically depicted in Fig. 15b, while an overview of the vacuum chamber and of the ink feeding-through system is given in Fig. 15c.

The ink was stored in a tank placed outside the vacuum chamber and it was fed inside by a proper liquid/gas feed-through. Inside the chamber a flexible pipe led the ink to the micro-valve. In this preliminary test the tank was kept at atmospheric pressure, then the feeding pressure was about 1 bar. Lower pressures might be required for future tests to improve the accuracy and resolution of the process. The final part of the nozzle, which had to be entirely inserted under the simulant surface, has an internal diameter of 0.8 mm, and is 8 mm long.

The regolith simulant was carefully mixed with 25% in weight of inorganic binder, then a 25 mm depth layer of this mixture was settled in the box and let in the test chamber, in vacuum conditions (pressure below 1×10^{-3} mbar), for about two days, so to perform an extensive outgassing of the air and water trapped inside the mixture grains. After this preliminary conditioning, the injection needle was inserted inside the mixture and a pressure in the range of 1×10^{-6} mbar was reached inside the vacuum chamber.

The test consisted in 6 ink injections, horizontally spaced by a few centimetres. At the starting position two brief shots were performed, in order remove the residual air that could be left inside the needle during the set-up activity. After the last injection, the simulant was left in vacuum condition for 24 h, in order to ensure the complete concretisation of the chemical reaction products. The 6 samples have been collected and measured after cleaning to remove the deposited unconsolidated material. Table 8 shows the masses of all the samples.

The relatively large mass of the last sample must be noticed, despite the valve opening time was quite the same of the other shots (see Fig. 16a). Furthermore, the last sample had an almost spherical shape. The reason for this anomaly lies in the fact that, after the last injection, the ink left in the volume between the valve and the end of the

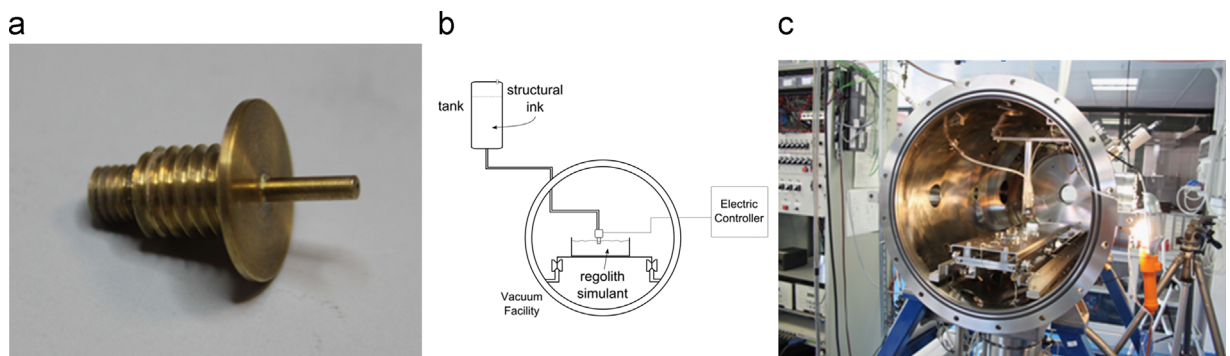


Fig. 15. (a) Injection nozzle, (b) test setup scheme and (c) IV 8 vacuum chamber and ink feeding-through system.

needle was slowly absorbed by the simulant, unlike in the previous shots. Finally sample no. 5 has been split to expose the internal structure, which is depicted in Fig. 16b. These results are encouraging, as they show that the reticulation process took place in vacuum and the obtained samples show promising structural behaviours.

6. Experiments with the D-shape technology applied to the regolith simulant

6.1. Mechanical characteristics of the material printed by using the regolith simulant

The D-shape binding chemistry exploits two inorganic reactants: the first one is a metallic oxide in powder form that is dispersed among the granular material and the powder component comprises at least one among Magnesium Oxide, Silicon Oxide, Iron Oxide, Calcium Oxide and Aluminium Oxide. In particular, the granular material is preferably selected from the group comprised of dolomite, calcareous which or siliceous sands to which Magnesium Oxide is added, in a ratio set between 15% and 30% by weight. Thus the first reactant is MgO, a white solid mineral that occurs in nature as periclase and is formed by an ionic bond between one magnesium and one oxygen atom. MgO is hygroscopic in nature and care must be taken to protect it from moisture. Magnesium hydroxide $Mg(OH)_2$ forms in the presence of water ($MgO + H_2O \rightarrow Mg(OH)_2$), but it can be reversed by heating it to separate moisture.

The second reactant is Magnesium Chloride, which is actually the generic name for the chemical com; pounds with the formulas $MgCl_2$ and its various hydrates $MgCl_2 \cdot (H_2O)_x$. These salts are typical ionic halides, being highly

soluble in water. The hydrated magnesium chloride can be extracted from brine or sea water. Magnesium Chloride as the natural mineral bischofite is also extracted (solution mining) out of ancient seabeds, such as, for instance, the Zechstein seabed in northwest Europe. In particular, in the standard D-shape printing process a saturated solution of Magnesium Chloride hexahydrate ($MgCl_2 \cdot 6H_2O$) (about 65%) is used, which is a Chlorine-based saturated salt solution characterised by a low viscosity.

When the two reactants are mixed together, an exothermic chemical reaction occurs generating a reticulating process which segregates in a matrix the granular material, with fibres eventually added to the mixture. At temperatures below 100 °C, the main composition phases produced in the ternary $MgO-MgCl_2-H_2O$ system are:

- $3Mg(OH)_2 \cdot MgCl_2 \cdot 8H_2O$ (Phase-3)
- $5Mg(OH)_2 \cdot MgCl_2 \cdot 8H_2O$ (Phase-5)
- $Mg(OH)_2$ (brucite).

This chemistry is known as Sorel cement. Magnesium-based Sorel cement was discovered in 1867. This mixture of magnesium oxide (burnt magnesia) with magnesium chloride has an approximate chemical formula given by $Mg_4Cl_2(OH)_6(H_2O)_8$, corresponding to a weight ratio of 2.5–3.5 parts MgO to one part $MgCl_2$. A variant uses Zinc Oxide with Zinc Chloride instead of the magnesium compounds. This cement has been used extensively, usually combined with filler materials such as sand or crushed stone, for industrial flooring, fire protection, grinding wheels and wall insulation, due to its superior mechanical and thermal properties, and even artificial ivory (e.g. for billiard-balls). In general, Sorel cement is very fast-setting and reaches very high compressive-strength (close to 10,000 psi, i.e. 70 MPa) within a few hours.

As the regolith simulant which has been adopted in the present experiments contains a quite high but insufficient amount of Magnesium Oxide to promote the chemical reaction with the structural ink, an addition of a mix of MgO (5% of the weight) has been performed, while the ink formulation remained unchanged with respect to the current applications of the process. In weight, the liquid binding solution can be considered composed of 23% of

Table 8
Masses of the extracted samples.

Sample	Mass (g)
1	0.75
2	0.14
3	0.30
4	0.25
5	0.75
6	1.11

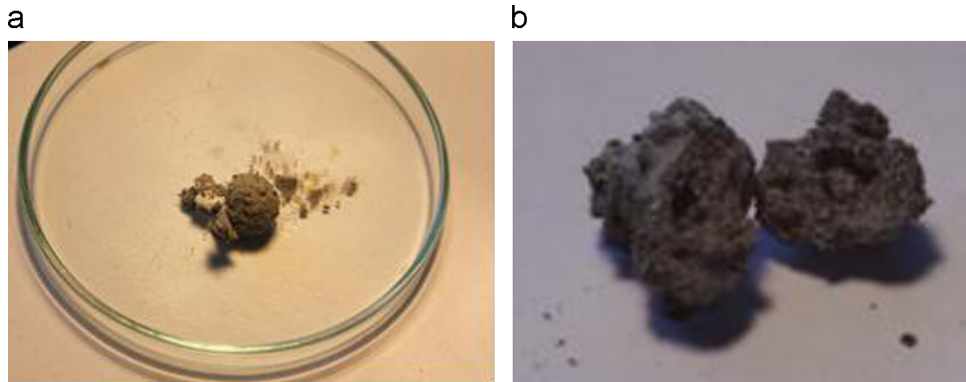


Fig. 16. (a) Sample no. 6 and (b) the internal structure of sample no. 5.

Table 9

Mechanical and physical properties of the D-shape processed stone specimens.

Ink property/content	Value	Unit of measure
Physical status	Slightly amber liquid	–
Odour	Odourless	–
pH	5–7	–
Density at 20 °C	1.288 ± 1.342	Kg/dm ³
% of Magnesium chloride hexahydrate (MgCl ₂ · 6H ₂ O)	64 ± 65	–
% of Magnesium chloride (MgCl ₂)	29.5 ± 31	–
% of Magnesium sulphate (MgSO ₄)	3.5 ± 4	–
% of Potassium chloride (KCl)	0.3 ± 0.4	–
% of Sodium chloride (NaCl)	0.05 ± 0.1	–
Boiling temperature	1.413	°C
Fusion point	714	°C

Table 10

Mechanical and physical properties of the D-shape processed stone specimens.

Property	Standard	Unit of measure	Value
Apparent density	UNI-EN 1936	Kg/m ³	1855.33
Apparent specific weight	UNE-EN-1936	Kg/m ³	2200
Total open porosity	UNI-EN-1936	%	13
Uniaxial compressive strength	EN 12390-3	N/mm ²	20.35
Compression resistance	UNE-EN-1926	Kg/cm ²	175–200
Bending resistance	UNE-EN-12372	Kg/cm ²	15–35
Young's modulus (E secant)	PrEN 14146	N/mm ²	2350
Poisson's ratio (Strain Gauge Method)	ASTM D3039/D3039M	N/mm ²	634.5
Flexural strength under concentrated load	UNE-EN 12372	N/mm ²	7.10
Linear thermal expansion coefficient	EN 14581-11	°C ⁻¹	68.3 × 10 ⁻⁶
Knoop microhardness	EN 14205	Kg/mm ²	145–250
Water absorption by capillarity	UNE-EN 1925	%	0.17
Freezing resistance	prEN 12371	Kg/cm ²	320–350
Resilience	EN 10545-5	Cm	50

dry salts and 77% of water. Further details on the ink are provided in Table 9.

The result is an artificial double magnesium-carbonate sand stone comparable to a dolomitic sand stone. The granulometry can be optimised to improve strength parameters for the final product, depending on the needs. Fibres and additional minerals can be also added to the mix to achieve better resilience and isotropic properties. The density of such mixed material is about 1.7 Tons/m³. This mix is non-toxic; however is recommended to manipulate it with gloves, glasses and masks. Moreover it requires to be stored into a low humidity room and used within 1 month from delivery, to save its catalysing properties.

The material produced by the D-shape process is a porous artificial sandstone which is anisotropic due to the layering process. Delamination problems can occur if the printing process is stopped and restarted later. Also the temperature or weathering of the reactants can affect the final quality of the produced stone. Table 10 provides a set of mechanical and physical properties from standard laboratory tests on a set of samples 'printed' with DNA regolith mixed with MgO, as above described.

6.2. Crystallographic analysis of the printed material

A crystallographic analysis through X-Ray Diffraction (XRD) has been pursued on the printed material in order to

find the major mineral species and compare them to those ones characterising the DNA-1 regolith samples and verify how the printing process interacts with the DNA-1 (and not only with the added amount of MgO) by eventually forming further mineralogical species. A Breg Brentano diffractometer has been used operating at 40 kV and 20 mA, exploiting a radiation Cu $\kappa\alpha$ with Ni filter. The results of such analysis is depicted in Fig. 17, where also the main mineralogical species which were pointed out are shown.

The analysis through X-ray diffraction is based on the fact that, when an appropriate electromagnetic wave impinges upon a crystal, an interference phenomena is observed, that is caused by the reflection of waves by different but parallel crystalline planes: from the angular position of the peak, using the following Bragg formula the inter-planar distance can be obtained which, compared with the values of the data base of the minerals, allows their detection [37]. The Bragg formula is given by:

$$n\lambda = 2d_{hkl} \cdot \sin(\theta) \quad (3)$$

where θ is the angle between the incident beam and the crystal plane, λ is the wavelength of the radiation, d_{hkl} is the distance between two adjacent planes and n is the diffraction order (usually $n=1$).

In Fig. 17 for each relevant peak the inter-planar distance expressed in Angstrom (\AA) is indicated as well as the corresponding mineral species. The crystallographic

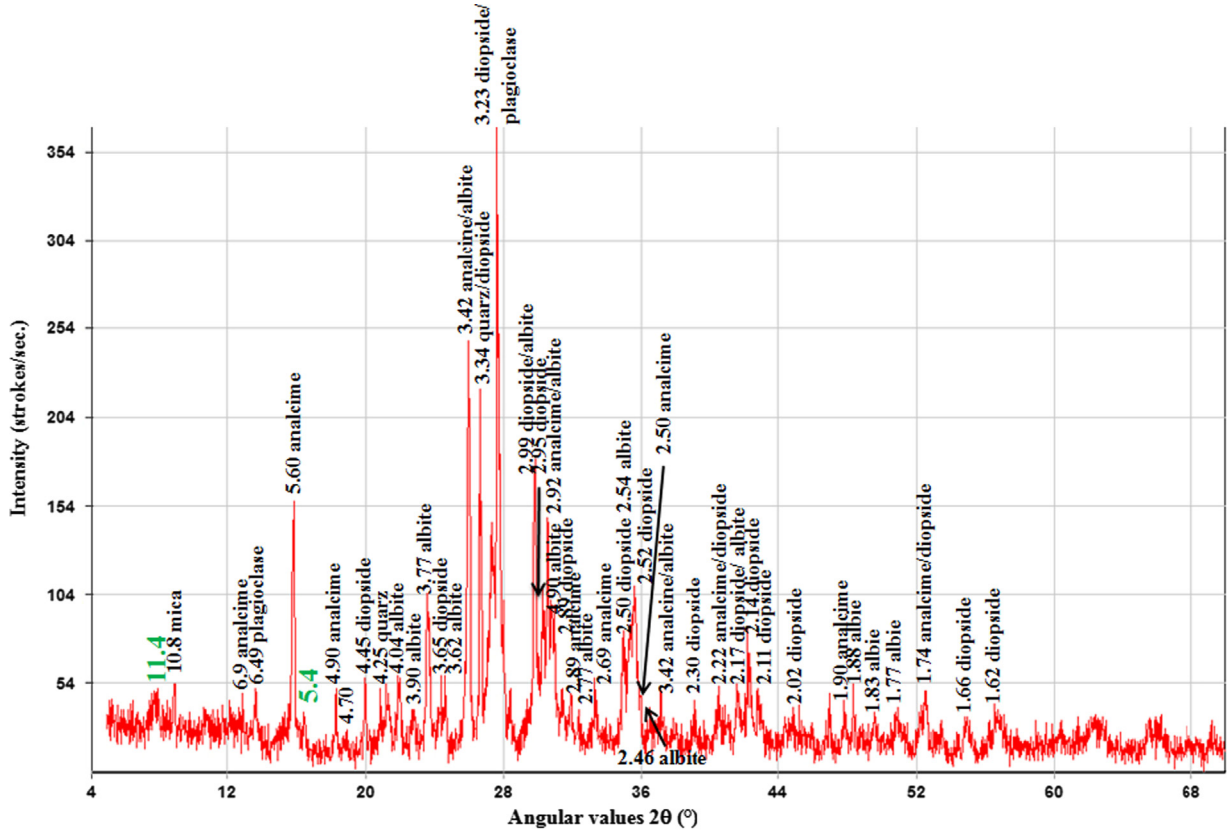


Fig. 17. X-ray diffraction spectrometry of a sample of the printed material.

analysis pointed out the presence of all the same mineral species that were also found in the DNA regolith simulant (see Table 7) but there also two ‘new’ weak traces corresponding to $d_{hkl}=11.4\text{ \AA}$ and $d_{hkl}=5.4\text{ \AA}$, that are highlighted in green color in Fig. 17. These values usually correspond to Calcium Silicate Hydrate (CSH) that can be formed as a consequence of the hydrothermal alteration of volcanic rocks, such as the ones that constitute the DNA regolith simulant.

The results of this analysis, on one hand, confirms the fact that the printing process basically involves the interaction between the MgO contained in the sand and the MgCl₂ contained in the ink, according to what is stated in Section 6.1, and the proportion between this two main components is the basis for making the printing process viable. On the other hand, the semi-qualitative nature of this analysis, does not allow to establish with certainty that during the printing process a reaction took place involving a small portion of the DNA regolith, but this cannot be excluded and thus will be the object of future deeper investigations.

6.3. Printing tests

The encouraging preliminary results obtained with DNA-1 regolith stimulant in vacuum condition, which are described in Section 5, made it meaningful to carry out some tests

where items of a significant size using the same simulant. Firstly a simpler item has been printed, to the aim of setting the printer parameters and provide useful design guidelines for the design of the final demonstrator. In this preliminary test, a convex artefact of a few centimetres thickness has been modelled at Dinitech (see Fig. 18a). The dimensions of this artefact, which is depicted in Figs. 18b and c, are 395 mm × 395 mm × 195 mm, while each layer has a depth of 5 mm, thus 39 layers are present. In order to build this preliminary demonstrator, about 100 kg DNA-1 were mined, milled to obtain a proper base material in terms of granulometry and mixed with MgO.

After this first experiment, some full scale demonstrators of the complex foam structure that has been selected as most promise solution for the external walls of the lunar outpost has been printed using the regolith simulant in atmosphere. Two demonstrators have been manufactured; the smallest one (Technical Demostrator no. 1—TD1) is 14.4 kg in weight, while the biggest (Technical Demonstrator no. 2—TD2) one is 1.3 tons in weight. Figs. 19 and 20 depict the two technical demonstrators that have been manufactured in the printing tests. In particular, the complex structural element reported in Fig. 6b is the same as the one depicted in Fig. 20.

Table 11 reports a comparison between the main geometrical and physical properties of TD1 versus the



Fig. 18. (a) 3D drawing of the convex artifact, (b) unpolished printed piece built using the DNA-1 simulant and (c) particular of the artifact surface after dust removal.

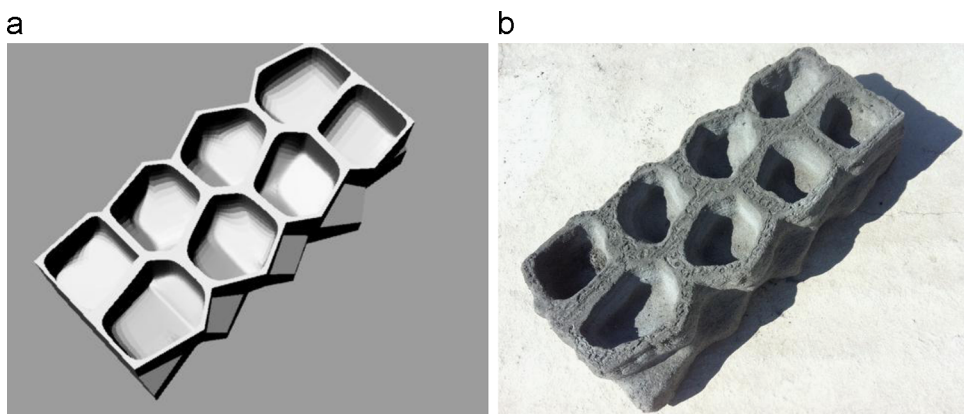


Fig. 19. The Technical Demonstrator no. 1: (a) CAD technical drawing and (b) the actual printed structural element



Fig. 20. The Technical Demonstrator no. 2, which is the structural element reported in Fig. 6b

design specifications (extracted by the CAD technical drawing) and the dimensions of the real printed block. The area of the printed demonstrator is very close to that specified by the design of the block. However, the average wall thickness of the printed block is far higher than specified inducing proportional increase in the weight of the demonstrator with respect to the design specifications.

The full-scale printing tests are very promising as all the geometrical features from the CAD model were well mimicked. However, the full scale printed demonstrators highlighted the shape accuracy limits of the current D-shape 3D printer.

It is expected that the discrepancies between design and actual hardware will be less pronounced in vacuum. Indeed, as reported above (see Section 5.2), the dimensions of the pebbles produced by reticulation tests under vacuum are close to that of the drop of liquid ink used to produce them. In air, the capillary forces driving the ink between regolith particles are not counterbalanced by the tendencies to boil or evaporate encountered in vacuum. Hence, it is more difficult to achieve tight dimensional tolerances.

To increase the shape accuracy of a next generation D-shape 3D printer, reduction of nozzle-diameter and appropriate tuning of ink volume release would need to be further investigated.

On a broader perspective, to establish the range of optimal parameters for using a 3D printer technology for lunar habitat a trade-off would be needed taking into consideration at least the building accuracy, the building rate and the amount of ink to be used.

7. Preliminary evaluation of transportation requirements and costs

A first very rough and preliminary estimate of the amount of material to be conveyed on the Moon have been attempted, based on the concept that basically only the inflatable inner core of the outpost and the dry salts for producing the binding material must be transported from

Table 11

Comparison between printed and designed versions of TD1.

Property	Unit	Symbol	A: Printed TD1	B: designed TD1	Ratio A/B
Volume	(mm ³)	V	8669476 $V=P/\rho b$	3140782 (From CAD)	2.76
Area	(mm ²)	A	660783 $A=V/t$	612995 (From CAD)	1.08
Average thickness	(mm)	T	13.12 (measured)	5.12 $t=V/A$	2.56
Density	(g/mm ³)	ρ_b	1.661×10^{-3} (measured)	1.661×10^{-3} (input into CAD)	1
Weight	(g)	P	14400 (measured)	5215 $P=V \times \rho_b$	2.761

the Earth, as the water is supposed to be found on the Moon and the Lunar soil contains enough MgO (see Table 6) that does not require any further addition. In fact, in a possible implementation scenario, there will surely be a transitory phase where the first habitation module will be built (possibly with the support of human operation) by producing the binding agent to feed the 3D printer inside the vessel that is used to bring to the Moon the printer itself, the inflatable structure, the salts, the machinery needed to extract water and all the rest of the required equipment. The first module will thus constitute a first 'in situ laboratory' where the material for building all the other outpost will be prepared, binding liquid to feed the printer included. At regime situation, the laboratory will be located inside one of the habitation modules and the machinery (printer, rovers and other equipment) will be already available on the Moon, thus finally only the dry salts for the binder and the inflatable structure will need to be transported. Future investigations should also further develop this concept and eventually minimise the volumes and weights of the material to be brought. For instance eventual further studies on the Moon rocks and soil might assess that the local production of the dry salts for the ink is viable, but presently few elements are available to state the actual feasibility of this solution.

Thus, in the above-described hypothesis, from the available dimensions of the outpost outer shell as described in Section 2.2 a total weight of about 250 tons has been estimated and 9.6% of this amount (i.e. 24 tons) is constituted of MgO. A rough estimate of the amount of sand to be dried with the ink is 30%, which corresponds to 75 tons of sand (of which 7.2 tons of MgO). The weight ratio between the dry salts contained in the ink and the MgO contained in the sand that was used to print the building blocks is approximately 0.53, thus about 3.8 tons of dry salts are needed to print the first outpost: as the salts density is about 1.6, thus this amount corresponds to a volume of 6 m³.

The inflatable structure can be approximated with a cylinder with a diameter of 2.5 m and a height of 8 m, which corresponds to a volume of 40 m³. Its weight can lie in the range between 1 and 1.5 tons.

The cost of a spatial mission is very variable and depends on the destination, the level of safety as a consequence of the possible presence of men on board and obviously on the weight and volume of the material conveyed on the spatial vessel. A reasonable figure for the amount of material that can be delivered on the Moon,

considering the requirements for ensuring safe landing for equipment and men, can lie in the range of 5–8 tons. As far as the volume of the material that can be transported, to the authors' knowledge the biggest space vector has a maximum length of 10.3 m and a diameter of 4.5 m, which corresponds to a rough overall volume of about 160 m³; thus a reasonable figure for the volume that can be conveyed in a single space vessel can lie in the range of 80–100 m³.

To sum up, considering both the above computed weight and volume of the raw material and the weight and volume of an ad-hoc designed version of the 3D printer, of the rovers and of other equipment, all the material that is needed to build the first lunar outpost (constituted by one dome) could be sent in one single (quite big) vessel. The cost per Kg of transported material is highly variable and can be considered as lying in the range between 40 and 400 k€/kg, thus the average value of 200 k€/kg can be considered. In the hypothesis of a delivery of 8 tons of equipment and material, a first and very rough estimate of the cost of the mission to build the first lunar outpost is 1600 M€.

An alternative could consist in sending a first small remote controlled or fully autonomous space vessel conveying enough material to build more than one single dome and a second mission with astronauts, vehicles and other equipment. The cost of this latter solution depends on the size of the two vessels and from a number of variables that makes such estimate very difficult.

All the above described reasoning constitutes a very rough estimate based on very simplified calculations, whose aim is just to show that in principle the investigated solution for the development of a lunar outpost is viable: further deep investigations and studies will be required to reach a real implementation stage for the design and realisation of a Lunar outpost, which will be the object of future work.

8. Conclusions

Moon colonisation will require the adoption of suitable techniques to build a manned outpost. The current study validated the concept of building some of its elements with the material that can be found on-site. Building using the in-situ resources should aim at providing protection from radiation, micro-meteoroids impacts, and thermal environment for the outpost on the Earth's natural satellite. In this paper, the main outcomes of a feasibility study

are provided concerning the exploitation of a particular 3D printing technology, the D-shape printer, for building infrastructure on the Moon using regolith.

This research work funded by the European Space Agency (ESA) was a multidisciplinary work bringing together complementary expertise and composed of many different phases:

- A preliminary design of the lunar outpost to be equipped with the consolidated regolith shield has been developed by Foster & Partners in close collaboration with Alta-Space.
- A suitable simulant of the lunar regolith has been developed to be used for the tests by Monolite. Alta Space verified that the D-shape process was working properly in vacuum and using a simulant of the lunar regolith by exploiting the natural physical properties (and, in particular, granulometry) of such material.
- The D-shape process has been tested in standard atmosphere for the construction of some demonstrator of building blocks of the lunar outpost with the regolith simulant, in order to prove that the required structural features of these particular blocks can be reproduced.

A further part of the research, which has not been treated here, concerned the development of concepts of the monitoring and control of the printing process, which can allow an early detection of malfunctioning and anomalous events by improving the system reliability and fault tolerance. The printer should come equipped with a robust control and monitoring system according to redundancy criteria and must be capable to fix errors, faults or other unpredicted events occurring during the printing process. To this aim, a preliminary study has been conducted which tested the application of a vision-based system (an industrial CCD camera with a 8 mm lens positioned above the structure, at 1.50 m from the ground floor, centred in the working area and directed perpendicular to the layer plane) and outlined some principles for exploitation of the information conveyed by the images. The basic idea for the monitoring is strictly linked to the nature of the layer-by-layer printing process and consists in capturing a 2D image of each layer and comparing it with the correspondent section of the desired 3D model. Part of the future work will deal with the further development of these monitoring concepts.

Finally an exercise has been performed (which is depicted in Fig. 1) for figuring out how a 'robotic' version of the D-shape printer could interact with other autonomous vehicles in order to build the lunar outpost. Obviously we are far from having solved all the problems related to the spatialisation of the D-shape technology, as this was beyond the scope of the project. Also the problem of reducing the dimensions of the printer and making it movable and fully controllable from remote will be the object of future work.

Although this study was only a preliminary feasibility study, the results are very promising and open the field to future deeper investigations aimed at building a real prototype of a printing machine to be sent on the moon.

Finally, the use of this kind of technology could eventually be extended to Martian applications, considering the composition of the base material plays a minor role in the working principles of the D-shape process.

Acknowledgements

This work has been developed within the project entitled '3D Printed building Blocks Using Lunar Soil' funded by the European Space Agency. The authors wish to thank for their precious contribution Leonardo Priami, Federico Cannelli and Stefano Caneschi of Alta, Fabio Ceccanti, who highly contributed to the research work for the period he was enroled at Alta, Scott Hovland from ESA who fed the team with his broad knowledge of space exploration requirements, Alice Borselli and Mirko Sgarbi of Scuola Superiore Sant'Anna.

References

- [1] D. Schulze-Makuch, L.N. Irwin, Optimizing space exploration, *Adv. Astrobiol. Biogeophys.* (2008) 203–241.
- [2] N. Ramachandran, A. Gale, Space colonisation, *Aerosp. Am.* 46 (12) (2008) 77.
- [3] G.R. Woodcock, Re-thinking Human Space Exploration, *AIAA Space 2009 Conference and Exposition*, Pasadena, CA (United States), September 14–17, 2009.
- [4] S. Raval, Exploration colonization resource extraction and utilization of Moon and Mars (ECROMM), in: *Proceedings of the 62nd International Astronautical Congress IAC*, Cape Town (South Africa) October 3–7 2011, vol. 9, 2011, pp. 7845–51.
- [5] A. Burelle, Mining the Moon: a first step in harnessing extraterrestrial resources, in: *Proceedings of the 61th International Astronautical Congress IAC 2010*, Prague, Czech Republic, September 27–October 1 2010, pp. 6914–18.
- [6] G. Madhavan Nair, K.R. Sridhara Murthi, M.Y.S. Prasad, Strategic, technological and ethical aspects of establishing colonies on Moon and Mars, *Acta. Astronaut.* 63 (11–12) (2008) 1337–1342.
- [7] L. Bell, Top-level considerations for planning lunar/planetary habitat structures, *J. Aerosp. Eng.* 24 (3) (2011) 349–360.
- [8] H.L. Litaker Jr., R.D. Archer, R. Szabo, E.S. Twyford, C.S. Conlee, R.L. Howard, Human habitation field study of the Habitat Demonstration Unit (HDU), *Acta Astronautica* 90 (2) (2013) 391–405.
- [9] T. Matula, K.A. Greene, Applying a design-to-evolve approach to early lunar settlements, *Earth and Space 2012*, in: *Proceedings of the 13th ASCE Aerospace Division Conference and the 5th NASA/ASCE Workshop on Granular Materials in Space Exploration*, 2012, pp. 1448–1457.
- [10] G.P. Merrill, *Rocks, Rock-Weathering and Soils*, MacMillan Company, New York, 1897.
- [11] F. Ceccanti, E. Dini, X. De Kestelier, V. Colla, L. Pambagian, 3D printing technology for a moon outpost exploiting lunar soil, in: *Proceedings of the 61th International Astronautical Congress IAC 2010*, Prague, Czech Republic, September 27–October 1 2010.
- [12] B. Sherwood, Decadal opportunities for space architects, *Acta. Astronaut.* 81 (2) (2012) 600–609.
- [13] J.F. De Weerd, M. Kruijff, W.J. Ockels, Search for Eternally Sunlit Areas at the Lunar South Pole from Recent Data, IAF 98-Q.07, 1998.
- [14] <http://www.esa.int/Our_Activities/Space_Engineering/Testing_Mars_and_Moon_soil_for_sheltering_astronauts_from_radiation>.
- [15] <http://www.nasa.gov/offices/oct/home/tech_life_settlement.html>.
- [16] A Mehta, G.C. Barker, The dynamics of sand, *Rep. Prog. Phys.* 57 (4) (1994) 383.
- [17] E.H. Lockwood, *The Tractrix and Catenary in A Book of Curves*, Cambridge University Press, Cambridge, UK, 1961 (ISBN 978-0-521-05585-7) (Chapter 13).
- [18] L.J. Gibson, M.F. Ashby, *Cellular Solids: Structure and Properties*, Cambridge Solid State Science Series, Cambridge University Press, Cambridge, UK, 1999. (ISBN 0-521-49560-1).
- [19] L.A. Haskin, P.H. Warren, *Lunar chemistry*, in: G.H. Heiken, D.T. Vaniman, B.M. French (Eds.), *Lunar Sourcebook*, Cambridge University Press New York, 1991, pp. 367–474.

- [20] Viewpoint monthly column: "Confused by Terminology?" Time-Compression Technologies, Wholers Associates Inc., March/April 2007 issue.
- [21] M.C. Metzger, B. Hohlweg-Majert, U. Schwarz, M. Teschnerb, B. Hammer, R. Schmelzeisen, Manufacturing splints for orthognathic surgery using a three-dimensional printer, *Oral Surg. Oral Med. Oral Pathol. Oral Radiol. Endodontol.* 105 (2) (2008) e1–e7.
- [22] P. Salvo, R. Raedt, E. Carrette, D. Schaubroeck, J. Vanfleteren, L. Cardon, A 3D printed dry electrode for ECG/EEG recording, *Sens. Actuators A: Phys.* 174 (2012) 96–102.
- [23] L.C. Ebert, M.J. Thali, S. Ross, Getting in touch—3D printing in Forensic Imaging, *Forensic Sci. Intl.* 211 (1–3) (2011) e1–e6.
- [24] D.T. Pham, S.S. Dimov, *Rapid Manufacturing: The Technologies and Applications of Rapid Prototyping and Rapid Tooling*, Springer-Verlag, New York, 2011 (ISBN 1-85233-360-X)bvv.
- [25] N. Hopkinson, P. Dickens, Emerging rapid manufacturing processes, in: N. Hopkinson, R. Hague, P. Dickens (Eds.), *Rapid Manufacturing: An Industrial Revolution for the Digital Age*, John Wiley & Sons Ltd., Chichester, W. Sussex, 2006, pp. 55–80. (ISBN 13 978-0-470-01613-8), (Chapter 5).
- [26] J. Gardiner, Sustainability and construction scale rapid manufacturing: a future for architecture and the building industry? Royal Melbourne Institute of Technology (RMIT), in: Proceedings of the 14th May Conference at Rapid 2009 Exhibition, Chicago—Illinois, 2009.
- [27] J. Pegna, Exploratory investigation of solid freeform construction, *Autom. Constr.* 5 (5) (1997) 427–437.
- [28] Lytle, et al., Adapting a teleoperated device for autonomous control using three-dimensional positioning sensors: experiences with the NIST RoboCrane, *Autom. Constr.* 13 (1) (2004) 101–118.
- [29] R.L. Williams II, J.S. Albus, R.V. Bostelman, Self-contained automated construction deposition system, *Autom. Constr.* 13 (3) (2004) 393–407.
- [30] Buswell, et al., Freeform construction: mega-scale rapid manufacturing for construction, *Autom. Constr.* 16 (2) (2007) 224–231.
- [31] B. Khoshnevis, et al., Lunar Contour Crafting—A Novel Technique for ISRU-Based Habitat Development, AIAA Conference, Reno (NV), January 2005.
- [32] B. Khoshnevis, D. Hwang, Contour crafting, a mega scale fabrication technology, *Manuf. Syst. Eng. Series* 6 (II) (2006) 221–251.
- [33] Buswell, et al., Design, data and process issues for mega-scale rapid manufacturing machines used for construction, *Automata. Construct* 17 (8) (2008) 923–929.
- [34] V. Colla, E. Dini, Large scale 3D printing: from Deep Sea to the Moon, in: "low-cost" 3D printing for science, education and sustainable development, in: E. Canessa, C. Fonda, M. Zennaro (Eds.), ICTP—The Abdus Salam Centre for Theoretical Physics, ICTP Science Dissemination Unit, 2013, pp. 127–132.
- [35] S.H. Masood, et al., Part build orientations based on volumetric error in fused deposition modelling, *Intl. J. Adv. Manufact. Tech* 16 (3) (2000) 162–168.
- [36] P.G. De Gennes, F. Brochard-Wyart, D. Quere, *Capillarity and Wetting Phenomena: Drops, Bubbles, Pearls*, 1st ed., Springer Science + Business Media, New York (USA,) 2004 (ISBN 0-387-00592-7).
- [37] J.M. Cowley, *Diffraction Physics*, North-Holland, Amsterdam, 1975.